DOI: 10.1002/ange.201001559

Nanostructures

Nanopeapods by Galvanic Displacement Reaction**

Carlos M. Hangarter, Young-In Lee, Sandra C. Hernandez, Yong-ho Choa, and Nosang V. Myung**

Nanoengineered materials with advanced architectures[1,2] are critical building blocks to modulate conventional material properties or amplify interface behavior for enhanced device performance. While several techniques exist for creating core/shell[3] and axial heterostructures,[4,5] complex configurations with discretely positioned particles within a wire or tube structure, deemed inorganic nanopeapods, have proved most challenging. Nanopeapods are comprised of a discontinuous interface system that has recently attracted attention for enhancement of thermoelectric, sensing, and photovoltaic characteristics with similar platforms. These features are a consequence of the difference in physical properties of the materials at the interfaces and confinement effects of the nanoparticles, which have the ability to cause biased scattering of photons and phonons, modulation of charge carrier mobility/concentration, and surface plasmon enhanced photocurrent.[6–9] Although nanopeapods have been fabricated by few different techniques, including specific scenarios[7] and more general routes,[10–13] common thermal activation processes such as solid-state reactions or Rayleigh instabilities require high temperature stability of the sheathing material and its immiscibility with embedded particles restricting the material set to noble metal peas and oxide pods. Annexing other inorganic nanopeapod materials (i.e. semiconductors, alloys, transition metals, etc.) would extend functionality and introduce a host of fundamentally important studies. Additionally, the possibility of tubes with embedded particles of the same composition or modulated nanowire/nanotube structures also offer an efficient route to study the effects of serial void formation[14] or tube wall confinement with mitigated contact issues and extreme precision.

The galvanic displacement reaction (GDR) has been used to create metal nanostructures with hollow interiors exhibiting a spectrum of geometries and multiwalled metal nanoshells.[15–18] Conversely, galvanic displacement has been implemented to coat Si with metal films/nanoparticles[19,20] and to generate compound semiconductor nanotubes from ferromagnetic nanowires.[21] However, to date this method has not been employed to selectively displace one component in bilayered nanowires to produce one-dimensional nanostructures with axial and radial composition modulation or to produce metal/semiconductor heterostructures, wherein one metal component is displaced by a semiconductor material and the other is retained. Thus, methodical incorporation of semiconductor nanomaterials with prearranged multilayered nanowires is a critical step, drastically augmenting the utility of galvanic displacement for synthesizing nanostructures.

Herein, galvanic displacement of electrodeposited multisegmented nanowires is reported as a novel method to achieve such nanopeapod structures at room temperature. This procedure exploits template-directed electrodeposition to fabricate segmented nanowires, providing a large material database to tune electrochemical potentials and the spacing precision of electrodeposition, which has been reported down to a few nanometers.[22] Since no heat treatment is required for this process, embedded particles can range from very thin disks to nanorods for geometric and direct interface manipulation. Additionally, more exotic shell materials are feasible for applications such as catalysis, nanomagnetism, sensors, and energy conversion. As proof of concept, Te nanotubes with embedded Au nanoparticles and $NiTe_{1.26}$ nanowires with embedded Au segments were fabricated by galvanic displacement reactions with distinct features to each, as these linear assemblages of nanoparticles are promising for plasmon waveguides.[23]

The driving force for GDR is the difference in redox potentials, a fundamental electrochemical process that is the basis of battery technology. The standard redox potentials[24,25] for the materials investigated herein are as given in Equation (1a–d).

$$Au^+ + e^- \rightarrow Au \qquad E^o = 1.83\ V_{NHE} \tag{1a}$$

$$HTeO_2^+ + 3H^+ + 4e^- \rightarrow Te + 2H_2O \qquad E^o = 0.551\ V_{NHE} \tag{1a}$$

$$Ni^{2+} + 2e^- \rightarrow Ni \qquad E^o = -0.257\ V_{NHE} \tag{1a}$$

$$Co^{2+} + 2e^- \rightarrow Co \qquad E^o = -0.277\ V_{NHE} \tag{1a}$$

The mechanism for creating hollow nanostructures by galvanic displacement reactions has been described previ-

[*] Dr. C. M. Hangarter, S. C. Hernandez, Prof. N. V. Myung
Department of Chemical and Environmental Engineering
University of California-Riverside
Riverside, CA 92521 (USA)
Fax: (+1) 951-827-7710
E-mail: myung@engr.ucr.edu
Homepage: http://www.engr.ucr.edu/~myung
Y.-I. Lee, Y.-h. Choa
Department of Fine Chemical Engineering
Hanyang University
Ansan 426-791 (Korea)
E-mail: choa15@hanyang.ac.kr

[**] This research work was supported by the Pioneer Research Center Program through the National Research Foundation of Korea (2010-0002231) funded by the Ministry of Education, Science and Technology (MEST) and the Fundamental R&D Program for Core Technology of Materials funded by the Ministry of Knowledge Economy, Republic of Korea.

Supporting information for this article is available on the WWW under http://dx.doi.org/10.1002/anie.201001559.

ously by Xia's group.[15] The generalized scheme starts with particle nucleation and growth of the more noble material on the surface of the sacrificial metal nanostructure, forming a thin, porous sheath. As the shell fills in, diffusion across the casing allows continued oxidation/dissolution of the sacrificial metal. The end result is a hollow nanostructure with an interior roughly resembling the exterior of the sacrificial metal (Scheme 1). A unique aspect of the bilayered nanowires

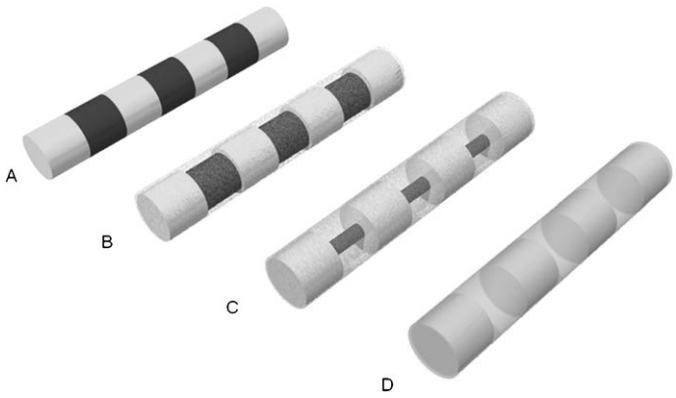

Scheme 1. Galvanic displacement reaction progression for Co/Au multisegmented nanowires. The as-synthesized Co/Au nanowire (A) is sheathed in a thin porous Te coating (B) that permits continued dissolution of the Co segments as the Te coating continues to grow (C) until the Te tube with embedded Au particles is all that remains (D).

is encapsulation of the more noble segment with the depositing material. This feature is a result of the receding base metal attached to the noble metal and their difference in electrochemical potentials. As a consequence, bilayers behave as conjoined electrodes of an electrochemical cell, with the noble particles serving as a cathode for reduction/deposition and the sacrificial metal as the oxidizing/dissolving anode. In individual nanowires the combined effect of displacement and the voltaic cell effect can be expected to produce a uniform coating along the length of the nanopeapod.

The initial Co/Au multilayered nanowires with alternating lengths of around 1.5 μm and 0.75 μm, respectively, and resulting construct with Co displacement by Te are shown in Figure 1. A distinct change in morphology after displacement indicates the entire structure has been coated. The rough surface of the Te tube with the nodular appearance in Figure 1B may be a consequence of surface roughness from the Co hydroxide/oxide layer (Figure S1 in the Supporting Information), which may impart some features of its topology onto the interior of the tube, or even the initial porosity that enables continued dissolution of the Co across the Te shell. However, similar morphological coatings on the Au segments suggest it may also be a result of the growth mechanism, which involves low nucleation and surface mobility. These are typical factors causing botryoidal deposits, suggesting that temperature may provide a means to improve crystallinity during displacement.[26] The transparency of Te allows the Au segments to be visually located with SEM and reveals a fairly consistent outer diameter for the Te nanotube, especially for coatings over the Au segments. The displacement of Co by Te

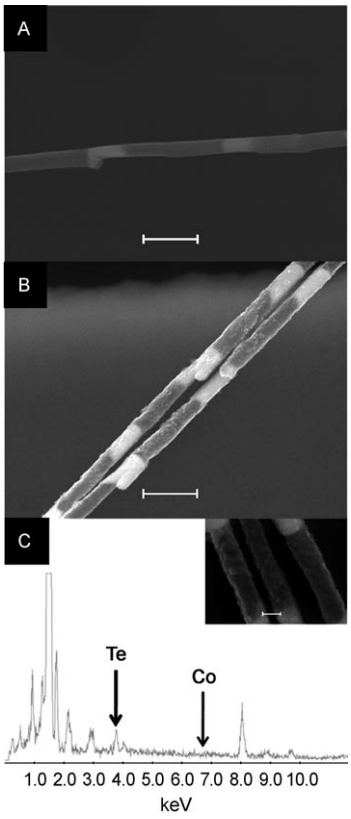

Figure 1. SEM images of A) electrodeposited Co/Au multisegmented nanowires and B) the corresponding Au/Te nanopeapod structure synthesized by galvanic displacement. Scale bars: 1 μm. C) EDX spectrum of image in inset indicating the presence of Te and no detectable concentration of Co. Scale bar: 1 μm (A,B), 200 nm (C, inset). Additional peaks pertain to the Au segments (2.12 keV) and substrate materials Cu (8.04 keV) and Al (1.48 keV).

after the galvanic displacement reaction was verified by energy dispersive X-ray spectroscopy (EDX). The EDX spectrum in Figure 1C indicates the absence of Co and the presence of Te. The TEM images in Figure 2 reveal the darker solid Au segments and Te tube cross section for different diameter nanowires. The enlarged image the Te tube segment, after displacement, reveals the granular structure with randomly oriented grains. The structure of the Te coating was verified by selected-area diffraction pattern (Figure 2A, inset), revealing a polycrystalline structure in agreement with similar results for Te nanotubes.[27] Although the structure is polycrystalline, refluxing at elevated temperatures may improve the crystallinity, in accord with the observed microstructure.[15] Additionally, the wall thickness ranges from 10 to about 27 nm with an inner diameter range from 225 to 250 nm. Recessed unions between the tube and Au core can be attributed to poor Co/Au interfaces, likely as a result of oxidation between depositions from rinsing and the nearly neutral pH Au sulfite bath. Interfacial quality can be improved by selection of an acid Au bath or a single bath with pulsed electrodeposition.[12]

Smaller Au/Te nanopeapod structures were also fabricated from polycarbonate templates. Although the nominal pore size diameters of these templates was 30 nm, the Au

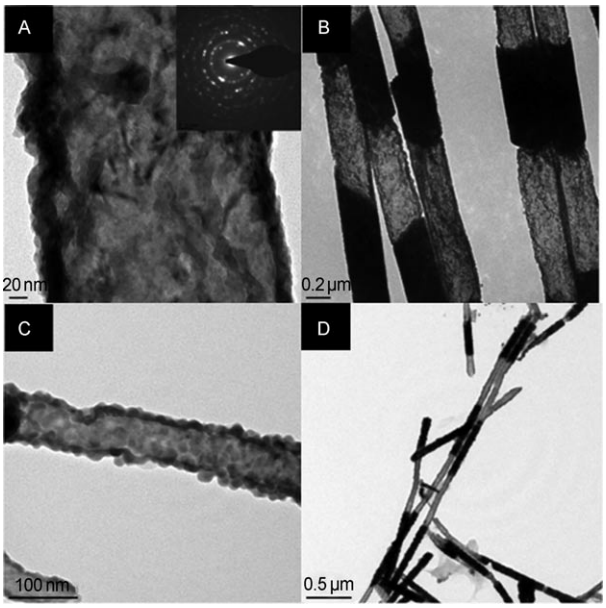

Figure 2. TEM image of a 300 nm diameter A) Te tube portion and B) full Te/Au nanopeapods. Inset: SAED pattern of the corresponding Te tube. C,D) TEM micrographs of 75 nm Te/Au nanopeapods produced from 30 nm pore size polycarbonate templates.

segments have a diameter of 65 nm. This discord in reported pore size to nanowire diameter (1:2.5) is typical of polycarbonate membranes and has been attributed to track etching and swelling.[27,28] The wall thickness of the Te tube in Figure 2C was measured to be approximately 12.5 nm with an outer diameter of 75 nm, indicating a slight contractions from the original Co segment diameter. This contraction is likely a consequence of the larger aspect ratio of the sacrificial Co segment, which is double that of the alumina template Co segment, permitting slight tube collapse prior to filling in. The decrease in wall thickness from the larger diameter Te/Au nanopeapod is in accord with the reduced volume of sacrificial Co. Moreover, the Te tube has a much more pronounced botryoidal microstructure, which also appears on the Au segment.

In contrast to Co/Au, Ni/Au multisegmented nanowires produced distinctly different nanopeapods consisting of wires with embedded Au segments. Ni/Au nanowires produced from alumina templates were poor candidates for GDR as the oxide and hydroxide layers from prolonged exposure to the template etchant (NaOH) passivated the surface, yielding inconsistent results. However, this issue was nullified with polycarbonate templates. The mechanistic nanopeapod formation described in Figure 1 was slightly modified to describe nanopeapods formed from Ni/Au nanowires. The kinetically slower displacement of Ni, which was shown to produce Te thin films at a rate half that of Co thin films, leads to a particle decorated intermediate. However, the etching rate of Ni in the nitric acid is still equivalent to that of Co, and thus creates a porous ligament or incomplete shell collapsing unto itself and forming a recessed wire with minimal deposit on the Au peas as a result of more significant etching of the sacrificial material.[24] This growth mechanism is consistent with the relative increased nobility of Ni with respect to Co, decreasing thermodynamic driving force for displacement, and the smaller grains sizes for galvanically synthesized Te from Ni are indicative of the slow growth rate.[24]

Representative SEM and TEM images of galvanic displaced Ni/Au multisegmented nanowires are shown in Figure 3. The sacrificial Ni/Au nanowires were approximately

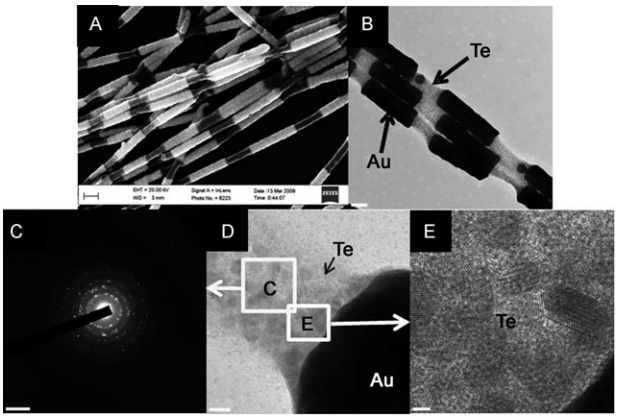

Figure 3. A) SEM image and B,D) brightfield TEM images of Ni/Au multisegmented nanowires synthesized from a 50 nm polycarbonate template after galvanic displacement. The SAED patterns in (C) correspond to the yellow box in (D) and the HRTEM image in (E) corresponds to the area mapped out by the white box in (D). Scale bars: A) 200 nm, B) 100 nm, D) 10 nm, and E) 2 nm.

115 nm in diameter and were grown from 50 nm polycarbonate templates. However, numerous variations of the Ni and Au segment lengths were investigated (see the Supporting Information for additional SEM and TEM results). The Ni segment appears to be etched to near completion, being replaced with well defined grains 2–8 nm large, embedded in an amorphous scaffold. Selected-area electron diffraction (SAED) patterns support a mixed polycrystalline/amorphous microstructure with d spacings (see Figure S3C in the Supporting Information) suggesting the presence of both monoclinic Te and rhombohedral NiTe, or possibly $NiTe_2$, as some lattice spacings clearly fit better to NiTe than Te. The gold segments display a predominately polycrystalline structure with larger grains relative to Te (see the Supporting Information). Contrary to Co/Au multisegmented nanowires, these samples displayed minimal Te deposition on the Au segments. EDX area mapping indicates uniform distribution of Ni and Te along the entire structure (Figure 4) with EDX spot analysis of the displaced nanowire segments indicating a composition of $NiTe_{1.26}$, corroborating SAED pattern d-spacing evidence for the presence of NiTe. The formation of the transition-metal chalcogenide NiTe is thermodynamically more favorable to Ni and Te because of its negative Gibbs free energy.[29] The reaction for NiTe formation is believed to occur topotactically after Te deposition by GDR. The nitrate complex of Ni^{2+} likely plays a crucial role similar to aqueous $AgNO_3$ used to create Ag_2Te and Ag_2Se materials from Te and Se nanowire precursors, respectively.[30,31] Dark-field images of these nanowires also

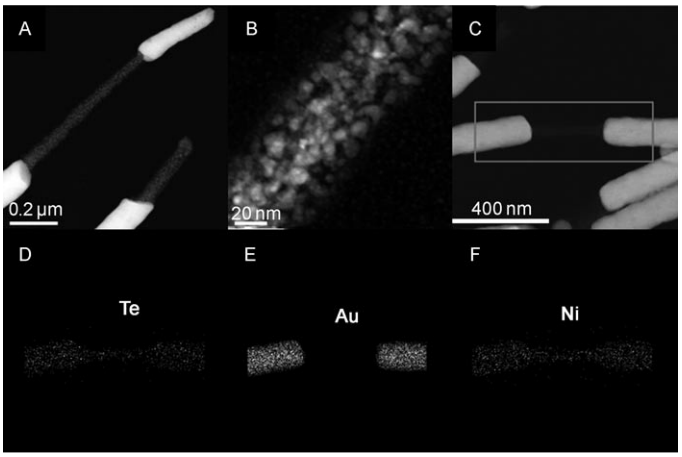

Figure 4. A–C) Darkfield TEM images of Ni/Au nanowires fabricated with 50 nm polycarbonate templates and subjected to galvanic displacement reaction with Te. The box in (C) indicates the area of the EDX mapping for D) Te, E) Au, and F) Ni.

highlight the granular structure of the Te segments and lack of hollow interiors (Figure 4).

The TEM images for nanowires fabricated from 30 nm polycarbonate membranes show the actual nanowire diameter to be approximately 75 nm. The Te/Au interface of a Ni/Au nanowire subjected to galvanic displacement reaction is shown in Figure 5. These wires appear very similar to those

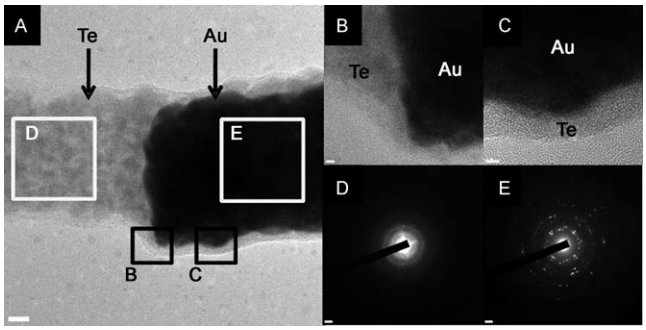

Figure 5. Brightfield TEM images of Ni/Au multisegmented nanowires from 30 nm polycarbonate template after galvanic displacement. The boxes in (A) correspond to the images in (B,C) and SAED patterns in (D,E). Scale bars: A) 10 and B,C) 2 nm.

fabricated from 50 nm polycarbonate membranes. The high-magnification TEM images show a granular structure for Te, but with comparably smaller and less lattice fringes, which agrees with the nearly amorphous SAED pattern (see Figure S5 in the Supporting Information). The Te coating on the Au segment is also more pronounced on these wires with thickness from 2 to 6 nm. Although the SAED pattern is nearly amorphous, two points are distinguishable and have very good d-space fittings to both Te and NiTe. This result supports the possibility of nickel chalcogenide formation (NiTe), but it is difficult to confirm this from the SAED pattern alone. The SAED pattern for the Au segments on these nanowires is similar to that of the previous nanowires, showing polycrystalline structure and d-spacing values except for a couple spots that can be attributed to the Te coating.

In conclusion, galvanic displacement was used to synthesize inorganic nanopeapods—one-dimensional nanostructures with both axial and radial composition modulation. This technique utilized bilayered nanowires with one sacrificial metal for galvanic displacement and a more noble material that is encapsulated during the process. The sacrificial metals produced distinctly different coatings from a Te tube to a NiTe alloy nanowire as a consequence of different redox potentials and a favorable topotactic reaction between the displaced material, Ni, and the deposited Te. SEM and TEM images revealed a botryoidal microstructure in the Te tubes, while the wires were composed of small grains embedded in an amorphous matrix. The Te coating over the Au was attributed to the difference in electrode potentials of the Au and sacrificial metal, allowing Au to mediate charge transfer from the sacrificial metal to $HTeO_2^+$. This approach is believed to be a general route to nanopeapod synthesis as numerous template-directed electrodeposition materials can be incorporated, including conducting polymers, magnetic materials, metal oxides, and compound semiconductors. Moreover, by exploiting the redox potential dependent reactions of galvanic displacement, nanopeapod materials can be extended (semiconductor/metal, p-type/n-type, metal/metal, ferromagnetic/nonmagnetic, etc.) to new and exotic nanopeapod materials. Finally, topotactic reactions may limit the selection of sacrificial materials but also provide a means for additional chemical transformation.[32]

Experimental Section

The procedure for fabricating nanopeapods follows that previously described for synthesizing Bi_2Te_3 nanotubes with the additional stipulation of a bilayer nanowire containing a base element for displacement and a more noble element that remains after the displacement reaction.[21] The segmented nanowires were synthesized by template-directed electrodeposition, a method pioneered by Martin and Moskovitz,[33,34] which uses a nanoporous template to confine electrodeposited material radially and the deposition condition to control the axial length of the nanowire. Alumina (Whatman Anodisk 13) templates and polycarbonate membranes (Nucleopore 30 and 50 nm) were sputtered with Au on one side using an EMS KX550 sputter coater. The sputtered Au acts as a seed layer for electrodeposition to proceed upon. Herein, alternating layers of Co/Au and Ni/Au were electrodeposited by a dual bath method at different diameters and lengths. After electrodeposition, the nanowires were harvested using 1M NaOH at room temperature to etch alumina templates and 1-methyl-2-pyrrolidinone at 50°C to dissolve polycarbonate membranes for 8 h each. The nanowires were washed three times by centrifuging or settling, extracting the supernatant, and then adding 18 MΩ cm water (Millipore A). Portions of nanowire batches were successively transferred to isopropyl alcohol (IPA) by a similar sequence of washings.

All nanowire electrodepositions were carried out in 100 mL electrochemical cells with a three-electrode configuration using a saturated calomel electrode (SCE) as a reference electrode. The Co electrolyte consisted of 1.0M $CoCl_2$ + 1.0M $CaCl_2$ at pH 4.0. Co electrodeposition was performed galvanostatically at $-10\,mA\,cm^{-2}$ and potentiostatically at −0.96 V (vs. SCE) at room temperature with

no agitation. The Au segments were electrodeposited from a sulfite-based commercial Technic bath (25 RTU-ES) containing 40 mM Au at a potential of −0.5 V (vs. SCE) or a current density of $-1\ mA\,cm^{-2}$ and a temperature of 50 °C with agitation from a 1 inch stir bar at 300 rpm. Synthesis of Ni/Au nanowires followed the same protocol as that of Co/Au nanowire synthesis. The Co electrolyte was simply substituted with a Ni electroplating bath. The composition of the bath was 1.5 M $Ni(NO_2SO_3)_2$ + 0.4 M H_3BO_3 + 0.2 M $NiCl_2$ at pH 4.0. H_3BO_3 was added as a buffer and $NiCl_2$ was used to enhance anode dissolution. Ni was electrodeposited galvanostatically at $-10\ mA\,cm^{-2}$ in a two-electrode configuration with a Ni counter electrode for alumina templates and potentiostatically in a three-electrode configuration at −0.96 (vs. SCE) for polycarbonate templates.

Galvanic displacement reactions were performed on both substrate bound nanowires and suspended nanowires. The substrate-bound nanowires employed Co/Au and Ni/Au multisegmented nanowires suspended in IPA, as the solvent evaporated quickly and provided good nanowire dispersion. The nanowires were cast on Si substrates ($0.25\ cm^2$) and allowed to dry. The substrate-bound nanowires were then submerged in 10 μL of the Te solution in nitric acid (1 M HNO_3 + 10 mM TeO_2) for 30 min. Following the displacement reaction, the solution was carefully wicked with a laboratory tissue and washed with a sequence of 10 μL droplets of 18 MΩ cm water on the substrate and wicking, three times each. Nanowires suspended in water were used for galvanic displacement in solution. The nanowire suspension (10 μL) was drawn and then dispensed in the Te solution (1 mL). The nanowires were immediately shaken to prevent agitation and to set aside for 30 min before washing three times with 18 MΩ cm water. SEM micrographs were taken with a Phillips XL30 FEG scanning electron microscope and an LEO Supra 55 scanning electron microscope. TEM micrographs were taken on C-coated Cu grids with a FEI Phillips CM300 transmission electron microscope.

Received: March 15, 2010
Revised: June 7, 2010
Published online: August 16, 2010

Keywords: electrochemistry · gold · nanostructures · nanotubes · tellurium

[1] W. K. Hong, J. I. Sohn, D. K. Hwang, S. S. Kwon, G. Jo, S. Song, S. M. Kim, H. J. Ko, S. J. Park, M. E. Welland, T. Lee, *Nano Lett.* **2008**, *8*, 950.
[2] Z. L. Xiao, C. Y. Han, W. K. Kwok, H. W. Wang, U. Welp, J. Wang, G. W. Crabtree, *J. Am. Chem. Soc.* **2004**, *126*, 2316.
[3] F. Qian, S. Gradecak, Y. Li, C. Y. Wen, C. M. Lieber, *Nano Lett.* **2005**, *5*, 2287.
[4] Y. Y. Wu, R. Fan, P. D. Yang, *Nano Lett.* **2002**, *2*, 83.
[5] B. Yoo, F. Xiao, K. N. Bozhilov, J. Herman, M. A. Ryan, N. V. Myung, *Adv. Mater.* **2007**, *19*, 296.
[6] M. S. Dresselhaus, G. Chen, M. Y. Tang, R. G. Yang, H. Lee, D. Z. Wang, Z. F. Ren, J. P. Fleurial, P. Gogna, *Adv. Mater.* **2007**, *19*, 1043.
[7] M. S. Hu, H. L. Chen, C. H. Shen, L. S. Hong, B. R. Huang, K. H. Chen, L. C. Chen, *Nat. Mater.* **2006**, *5*, 102.
[8] W. Kim, J. Zide, A. Gossard, D. Klenov, S. Stemmer, A. Shakouri, A. Majumdar, *Phys. Rev. Lett.* **2006**, *96*, 045901.
[9] S. Mubeen, T. Zhang, B. Yoo, M. A. Deshusses, N. V. Myung, *J. Phys. Chem. C* **2007**, *111*, 6321.
[10] J. A. Sioss, C. D. Keating, *Nano Lett.* **2005**, *5*, 1779.
[11] Y. Qin, L. F. Liu, R. B. Yang, U. Gosele, M. Knez, *Nano Lett.* **2008**, *8*, 3221.
[12] L. F. Liu, W. Lee, R. Scholz, E. Pippel, U. Gosele, *Angew. Chem.* **2008**, *120*, 7112; *Angew. Chem. Int. Ed.* **2008**, *47*, 7004.
[13] Y. Qin, S. M. Lee, A. Pan, U. Gosele, M. Knez, *Nano Lett.* **2008**, *8*, 114.
[14] S. Meister, D. T. Schoen, M. A. Topinka, A. M. Minor, Y. Cui, *Nano Lett.* **2008**, *8*, 4562.
[15] Y. G. Sun, B. T. Mayers, Y. N. Xia, *Nano Lett.* **2002**, *2*, 481.
[16] Y. G. Sun, B. Mayers, Y. N. Xia, *Adv. Mater.* **2003**, *15*, 641.
[17] Y. G. Sun, B. Wiley, Z. Y. Li, Y. N. Xia, *J. Am. Chem. Soc.* **2004**, *126*, 9399.
[18] Y. G. Sun, Y. N. Xia, *Adv. Mater.* **2004**, *16*, 264.
[19] C. P. daRosa, R. Maboudian, E. Iglesia, *J. Electrochem. Soc.* **2008**, *155*, E70.
[20] A. Gutes, I. Laboriante, C. Carraro, R. Maboudian, *J. Phys. Chem. C* **2009**, *113*, 16939.
[21] F. Xiao, B. Yoo, K. H. Lee, N. V. Myung, *J. Am. Chem. Soc.* **2007**, *129*, 10068.
[22] L. D. Qin, S. Park, L. Huang, C. A. Mirkin, *Science* **2005**, *309*, 113.
[23] S. A. Maier, P. G. Kik, H. A. Atwater, S. Meltzer, E. Harel, B. E. Koel, A. A. G. Requicha, *Nat. Mater.* **2003**, *2*, 229.
[24] C. H. Chang, Y. Rheem, Y. H. Choa, D. H. Shin, D. Y. Park, N. V. Myung, *Electrochim. Acta* **2010**, *55*, 743.
[25] A. J. Bard, L. R. Faulkner, *Electrochemical Methods: Fundamentals and Applications*, 2nd ed., Wiley, New York, **2001**, appendix C.
[26] R. F. Bunshah, *Deposition technologies for films and coatings: developments and applications*, Noyes Publications, Park Ridge, NJ, USA, **1982**.
[27] Y. Rheem, C. H. Chang, K.-H. Lee, C. M. Hangarter, N. V. Myung, *Electrochim. Acta* **2009**, *55*, 2472.
[28] C. Schönenberger, B. M. I. vanderZande, L. G. J. Fokkink, M. Henny, C. Schmid, M. Kruger, A. Bachtold, R. Huber, H. Birk, U. Staufer, *J. Phys. Chem. B* **1997**, *101*, 5497.
[29] M. S. Baba, R. Viswanathan, C. K. Mathews, *Rapid Commun. Mass Spectrom.* **1996**, *10*, 691.
[30] A. K. Samal, T. Pradeep, *J. Phys. Chem. C* **2009**, *113*, 13539.
[31] B. Gates, B. Mayers, Y. Y. Wu, Y. G. Sun, B. Cattle, P. D. Yang, Y. N. Xia, *Adv. Funct. Mater.* **2002**, *12*, 679.
[32] G. D. Moon, S. Ko, Y. Xia, U. Jeong, *Acs Nano* **2010**, *4*, 2307.
[33] C. R. Martin, *Science* **1994**, *266*, 1961.
[34] D. Al-Mawlawi, C. Z. Liu, M. Moskovits, *J. Mater. Res.* **1994**, *9*, 1014.

